# Molecular imaging of innate immune cell function in transplant rejection

Published in final edited form as:
*Circulation*. 2009 April 14; 119(14): 1925–1932. doi:10.1161/CIRCULATIONAHA.108.796888.

# Molecular imaging of innate immune cell function in transplant rejection

**Thomas Christen, MD, PhD**[*], **Matthias Nahrendorf, MD, PhD**[*], **Moritz Wildgruber, MD**, **Filip K. Swirski, PhD**, **Elena Aikawa, MD, PhD**, **Peter Waterman, BS**, **Koichi Shimizu, MD, PhD**, **Ralph Weissleder, MD, PhD**, and **Peter Libby, MD**

*Cardiovascular Division, Department of Medicine, Brigham and Women's Hospital, Boston, MA (T.C., K.S., P.L.), Center for Systems Biology, Massachusetts General Hospital, Boston, MA (M.N., P.W., R.W.) and Department of Systems Biology, Harvard Medical School, Boston, MA (RW), Center for Molecular Imaging Research, Massachusetts General Hospital, and Harvard Medical School, Charlestown, MA (M.N., E.A., M.W., F.K.S., P.W., Y.I., R.W.)*

## Abstract

**Background—**Clinical detection of transplant rejection by repeated endomyocardial biopsy requires catheterization and entails risks. Recently developed molecular and cellular imaging techniques that visualize macrophage host responses could provide a noninvasive alternative. Yet, which macrophage functions may provide useful markers for detecting parenchymal rejection remains uncertain.

**Methods and Results—**We transplanted isografts from B6 mice and allografts from Balb/c mice heterotopically into B6 recipients. In this allograft across major histocompatability barriers, the transplanted heart undergoes predictable progressive rejection leading to graft failure after 1 week. During rejection, crucial macrophage functions including phagocytosis and release of proteases render these abundant innate immune cells attractive imaging targets. Two or six days after transplantation, we injected either a fluorescent protease sensor or a magneto-fluorescent phagocytosis marker. Histological and flow cytometric analyses established that macrophages function as the major cellular signal source. In vivo, we obtained a 3D functional map of macrophages showing higher phagocytic uptake of magneto-fluorescent nanoparticles during rejection using MRI and higher protease activity in allografts than in isografts using tomographic fluorescence. We further assessed the sensitivity of imaging to detect the degree of rejection. In vivo imaging of macrophage response correlated closely with gradually increasing allograft rejection and attenuated rejection in recipients with a genetically impaired immune response resulting from a deficiency in recombinase-1 ($RAG\text{-}1^{-/-}$).

**Conclusions—**Molecular imaging reporters of either phagocytosis or protease activity can detect cardiac allograft rejection noninvasively, promise to enhance the search for novel tolerance-inducing strategies, and have translational potential.

### Keywords

leukocytes; inflammation; transplantation; rejection; imaging

Corresponding author: Peter Libby, MD, Brigham and Women's Hospital, NRB 741, 77 Avenue Louis Pasteur, Boston, MA, 02115, USA, Phone: 617 525-4350, Fax: 617 525-4999, E-mail: E-mail: plibby@rics.bwh.harvard.edu.
[*]authors contributed equally to this work

**Disclosures:** Ralph Weissleder is shareholder of Visen Medical.

## Introduction

Acute parenchymal rejection causes most graft failure in the first year after heart transplantation and rejection episodes predispose to the development of chronic allograft vasculopathy [1, 2]. Thus, close surveillance of transplanted organs remains mandatory. The current clinical standard of repetitive invasive endomyocardial biopsies is prone to sampling error, entails a risk of complication, and causes discomfort and anxiety for the patients [3]. Therefore, developing noninvasive yet quantitative diagnostic tools to monitor parenchymal allograft rejection would fulfill a compelling need.

T cells orchestrate allograft rejection; however, macrophages (MΦ) represent an abundant innate immune cell type in these allografts. Various roles of MΦ emerge in ischemia-reperfusion injury (IRI) and in the alloimmune reaction [4]. Whereas in IRI, macrophages function as major effector cells in the inflammatory response during the reperfusion phase, in the allogenic response their functions include facilitating adaptive immunity as antigen-presenting cells, contributing to cell and tissue damage as inflammatory effector cells, and promoting healing and repair once the graft recovers from acute insults [5]. The large number of MΦ and the key role of their effector functions during rejection, which include phagocytosis and release of proteases, render them attractive molecular imaging targets.

Recently developed probes report on different biological functions including phagocytosis and protease activity [6, 7]. Yet, it remains uncertain which probes best detect and quantify the MΦ response during parenchymal rejection. In this study we co-injected a quenched fluorescent substrate reporter for cathepsin proteases (protease sensor) and a nanoparticle-based phagocytosis sensor, choosing these probes for their robustness, clinical translatability, and ease of use in multimodality imaging. Capitalizing on the fluorescent properties of both probes, we compared the cellular contribution profile of the signal by flow cytometry analysis of digested heart grafts and its correlation with immunohistochemical staining — the reference standard — and investigated the ability of the different probes to render a three-dimensional functional map of macrophage localization. Finally, we assessed the capacity of MΦ-targeted imaging to resolve a genetically-impaired immune response by use of recipients with recombinase-1 deficiency.

## Materials and methods

### Animals

8-12 weeks old inbred male C57BL/6 (B/6, H-2b), BALB/c (B/c, H-2d), and RAG1$^{-/-}$ (B/6 background, H-2b) mice were obtained from Jackson Laboratory (Bar Harbor, ME). The mice were maintained at the animal facilities of Brigham and Women's Hospital, Massachusetts General Hospital, and Harvard Medical School, accredited by the American Association of Laboratory Animal Care. All experiments conformed to animal care protocols approved by the institutional review board. Figure 1 depicts the experimental protocol.

### Heterotopic cardiac transplantation

Iso- (B/6) or allografts (BALB/c) were heterotopically transplanted into B6 wild type or RAG1$^{-/-}$ recipient mice in an infrarenal location as described in the online data supplement. In sham-operated mice, we dissected the infrarenal aorta and inferior vena cava and after clamping these two vessels for an hour, we restored blood flow and closed the incision.

### Immunohistochemistry

We performed immunohistochemical staining as specified in the online data supplement. For quantification, numbers of positive cells in 20-30 high-magnification fields were averaged on transverse sections of the donor heart.

### Flow cytometry

Following euthanasia, we processed samples of the donor heart for flow cytometric analysis as described in the online data supplement. For each sample, 100,000 events were collected. Total number of cell types was determined by multiplying the total cell number per mg tissue (obtained with Trypan blue) by the percentage of a given cell type within the living gate (obtained with flow cytometry). Data were acquired on an LSRII device (BD Biosciences). To detect Prosense-680 or CLIO-VT680, samples were excited with the red laser (635 nm) and detected with 685/LP and 695/40 filter configuration.

### Nanoparticles and imaging

The following two imaging agents were co-injected into the tail vein 24 hours before in vivo fluorescence molecular tomography (FMT) and MR imaging: ProSense-680 (excitation wavelength 680±10 nm, emission 700±10 nm) [8] for imaging of the protease activity, 5 nmol in 150 μL PBS, and CLIO-VT750 nanoparticles (excitation wavelength 750±10 nm, emission 780±10 nm) [9] for imaging of the phagocytic activity, 15 mg of Fe/kg bodyweight. For flow cytometry, we injected ProSense-680 or CLIO-VT680 nanoparticles.

FMT was performed on a dual channel imaging system (FMT 2500, VisEn Medical, Woburn, MA) as previously described [106].

MRI studies were performed using a 7 Tesla horizontal bore scanner (Bruker Pharmascan, Billerica, MA) after injection of the phagocytosis sensor and following a protocol described in the online data supplement. The contrast-to-noise ratio (CNR) between the myocardium and the skeletal muscle was calculated as follows: CNR = (myocardial signal − skeletal muscle signal) / (standard deviation of the noise).

After euthanasia, native hearts and donor heart were excised and sections visualized using a custom-built fluorescence reflectance imaging (FRI) system (BonSAI Siemens, [11]) as detailed in the online data supplement.

### Statistics

Data are reported as mean ± SEM. When comparing two groups, we used Student's *t* test and for multiple comparisons we used ANOVA with subsequent Bonferroni correction. Differences, indicated by an asterisk, were considered statistically significant at $p < 0.05$. We performed statistical analysis with GraphPad Prism 4.0c for Macintosh (GraphPad Software, Inc, San Diego, Calif).

### Statement of responsibility

The authors had full access to and take full responsibility for the integrity of the data. All authors have read and agree to the manuscript as written.

## Results

### Macrophages and cathepsin-expressing cells accumulate abundantly in rejecting cardiac allografts

As in human heart transplantation, allografting in mice requires periods of warm and cold ischemia, conditions that can provoke non-immunological parenchymal injury. Study of isografts permits isolation of the consequences of ischemia-reperfusion from immunologically mediated tissue damage [12]. Our prior studies have described in detail the cellular and inflammatory sequences of events in hearts allografted under these conditions [4, 13]. Here we performed immunohistochemistry to define not only the sequence of inflammatory cell accumulation in heart grafts but also to quantify macrophages and cathepsin-expressing cell in these allografts. Analysis of the sections stained with anti-mac3, anti-NIMP-R14, anti-CD4, anti-CD8, anti-cathepsin B, and anti-cathepsin S of iso- and allografts at postoperative day (POD) 3 and 7 indicated the number of positive cells (Figure 2). This technique detected only a few neutrophils in the heart grafts at POD 3 and 7, with no difference among groups. Macrophages, abundant innate immune cells and important amplifiers of T cell driven response in graft rejection, accumulated predominantly in the allografts over time. As expected, CD4 and CD8 T lymphocytes accumulated almost exclusively in the allografts, but later and to a lesser extent than did macrophages. Inflammatory cells in the graft expressed both cathepsins B and S, and the allografts had more protease-positive cells than did the isografts.

### Fluorescent signals from both probes colocalize with immunoreactive macrophages and cathepsin B

After co-injection of the fluorescent sensor reporting on protease activity and a magneto-fluorescent phagocytosis sensor, we assessed the fluorescent signal by microscopy at different wavelengths on the same section of heart grafts. In the 680-nm channel, the Prosense-derived fluorescence signal colocalized with positive staining for cathepsin B and cathepsin S as well as macrophages (Figure 3 A, B, C, E). In the channel for the CLIO-VT750 emission, the signal also colocalized with macrophages (Figure 3 C, E). Neutrophils (sparse in the myocardium and mainly accumulating in the left ventricular thrombus) and non-hematopoietic cells did not colocalize with the fluorescent activity (data not shown). Acquiring images in the FITC channel facilitated the conclusion that autofluorescence contributes negligibly to the fluorescent signal in the channels specific for each probe (Figure 3 F).

### Macrophages: the major cellular source for the fluorescent signal

Determining how different inflammatory cell populations contributed to the overall fluorescent signal entailed flow cytometry with single-cell suspensions of digested donor hearts. First, using specific antibodies, we separated and visualized the cell populations of monocytes/macrophages, neutrophils, and CD11b negative cells (Figure 4 A). Second, after gating on specific cell populations, determination of staining intensities occurred after either protease sensor or phagocytosis sensor injection (Figure 4 A). At POD 7, allografts from animals injected with the phagocytosis sensor had markedly higher staining intensity and more monocytes/macrophages than did isografts, with protease sensor injection producing a similar result (Figure 4 A). Third, the representation of the relative contribution of each cell population to the overall fluorescent signal illustrated that although the monocyte/macrophage population comprised the major cellular contributor in most groups, neutrophils and non-myeloid cells or CD11b negative cells also contributed to the signal (Figure 4 B, C). The area of the pie charts indicates the total fluorescence signal in a given group and revealed a higher signal in allografts than in isografts at POD 7 (Figure 4 C).

### Allografts exhibit higher overall protease activity

After defining cellular and biological characteristics of the protease sensor, we explored its ability to detect the expected difference in inflammatory activity between isografts (B6 into B6) and allografts (Balb/c into B6) in vivo. We assessed the protease activity after protease sensor injection using fluorescence molecular tomography (FMT) at POD 3 and 7. At POD 7, allografts showed higher fluorescence than isografts, and the signal emanating from the allografts increased from day 3 to day 7 (Figure 5 A, B, C). We used two control groups: 1) sham-operated mice, which showed only background signal (Figure 5 C); and 2) native hearts in the same mouse showing only minimal fluorescence (data not shown). Fluorescence measured by FMT correlated with the number of macrophages enumerated by histologic examination ($R^2$=0.42, p=0.0014; Figure 5 D) and cellular staining for cathepsins B and S (data not shown). Fluorescence reflectance imaging (FRI) of excised myocardial rings at POD 3 and 7 supported these in vivo results (Figure 5 E, F, G). Heart slices from allografts had higher reflected fluorescence at POD 7 than did those from isografts (Figure 5 F and E), while the native hearts of the same animals had very low reflected fluorescence (insets in Figure 5 F and E). The counts per pixel detected from a myocardial ring of the donor heart were normalized to the counts of the native heart in the same animal (Figure 5 G). A gradual increase in the target-to-background ratio (TBR) in allografts and a lower TBR in the isograft compared to the allograft corroborated the in vivo FMT data.

### Higher Phagocytic activity in allografts than in isografts

To evaluate the capacity of the magneto-fluorescent nanoparticle to resolve phagocytic activity between allografts and isografts, we performed MRI at POD 3 and 7 in animals injected with the phagocytosis sensor. To gate acquisition selectively for the intra-abdominal donor heart ECG, leads were placed on the hind limbs (Figure 6 B). In T2* weighted sequences, nanoparticle uptake in the donor heart resulted in a higher contrast-to-noise ratio (CNR) in allografts than in isografts at POD 7 and an increase in CNR in allografts from POD 3 to POD 7 (Figure 6 E, F, G). Exploiting the optical properties of the magneto-fluorescent nanoparticle, we carried out FRI, and myocardial rings from allografts had higher fluorescence signals than those from isografts at POD 7, and in allografts the reflected fluorescence increased with time (Figure 6, H, I, K). MRI and FRI after phagocytosis sensor injection at POD3 (when ischemia-reperfusion injury has not waned and parenchymal rejection has not peaked) did not yield significant differences between iso- and allografts.

### Imaging signal intensity in allografts reports on magnitude of allograft rejection

To demonstrate that the signal intensity (pmol fluorescence for FMT and CNR for MRI) arising from in vivo imaging approaches reflects the severity of the immune response, we compared protease activity and phagocytosis in allografts of B6 wild-type recipients at POD 3 and 7 with grafts implanted into genetically immunodeficient $RAG1^{-/-}$ mice, which lack mature T and B cells. In vivo assessment by FMT showed not only increasing fluorescence in B6 wild-type recipients from POD 3 to POD 7 but also a lower imaging signal in $RAG1^{-/-}$ recipients than in B6 wild-type recipients at POD 7 (Figure 7 A). Similarly, evaluating the phagocytic activity with in vivo MR imaging showed that CNR of allografts in B6 wild-type recipients intensified with time whereas grafts in $RAG1^{-/-}$ recipients had a lower CNR than those in B6 wild-type recipients at POD 7 (Figure 7 B). Ex vivo FRI corroborated these findings after protease sensor (Figure 7 C) and phagocytosis sensor injection (Figure 7 D). Likewise, for both probes, flow cytometry (Figure 7 E) and immunohistochemical study (Figure 7 F, G, and H) validated these imaging results. Finally, to link further the in vivo imaging signal to the magnitude of rejection, we show correlations between phagocytosis as assessed by MRI and number of macrophages obtained from histological enumeration (Figure 7 I, $r^2$=0.85, p=0.001) as well as between

protease activity as assessed by FMT and cellular cathepsin B staining (Figure 7 K, $r^2$=0.33, p=0.006).

## Discussion

The clinical diagnosis of cardiac allograft rejection currently requires invasive biopsy and histological examination based on morphological rather than functional criteria. Macrophages, increasingly recognized as key inflammatory amplifiers in T cell-driven organ rejection [5], comprise a large part of the cellular infiltrate during rejection. Their phagocytic activity and protease expression participate in tissue damage and graft rejection, rendering them attractive targets for functional imaging. This study compared the ability of two different imaging probes to report on these key macrophage functions. By exploiting the fluorescent capacities of both imaging probes we assessed the detailed cellular contribution profile and identified macrophages as the major cell type responsible for protease sensor activation and uptake of the phagocytosis sensor. In vivo, imaging with both probes provided a functional three-dimensional map of macrophage accumulation, allowing detection of parenchymal rejection. Finally, the sensitivity of our optical and magnetic resonance imaging approaches enabled us to detect gradually advancing graft rejection in allografts as well as diminished accumulation of inflammatory cells and decreased protease activity in RAG1$^{-/-}$ allograft recipients, a situation of attenuated rejection. Thus, probes reporting on both protease activity and phagocytosis allow detection of parenchymal rejection, and these imaging approaches that interrogate macrophage functions during rejection could permit investigative evaluation of novel therapeutic strategies and the longitudinal assessment of individualized immunosuppressive regimens.

In the classical sequence of inflammatory cell accumulation in solid organ allografts, neutrophils arrive early and disappear first [14], followed by macrophages, present throughout the life of the graft, in the company of the CD4 and CD8 T lymphocytes. While studies have reported the presence of different cathepsins in animal and clinical studies in transplantation research, their roles remain largely unknown [15, 16]. In our study, immunostaining not only defined the differences in macrophage accumulation and cathepsin staining between iso- and allografts but also the relative abundance of macrophages in allografts, highlighting their appeal as target cells.

To explore the cellular and molecular distribution of the protease sensor and the phagocytosis sensor in the grafted hearts, we took advantage of their fluorescent moieties. The fluorescent signal of both probes colocalized microscopically with cathepsins B and S as well as Mac-3 staining, suggesting that macrophages predominantly activate the protease sensor and internalize the nanoparticle. Stronger fluorescence emanated from the protease sensor than from the phagocytosis sensor, possibly because one molecule of protease can cleave multiple molecules of the protease sensor, resulting in signal amplification. To profile the cellular signal distribution, we performed flow cytometry, which established macrophages as the major cellular contributor to the imaging signal for both probes. As previously reported, the contribution of neutrophils decreased over time with waning ischemia-related injury [14]. CD11b negative or non-myeloid cell populations contributed negligibly to the signal (between 5-7% in allografts at POD7). This heterogeneous cell population includes not only lymphocytes but most likely also stromal vascular cells, and low uptake of this phagocytosis reporter by non-“professional” phagocytes can occur [17]. Finally, the fluorescent features of both probes revealed that while the protease sensor seems to target macrophages more specifically than the phagocytosis sensor (81 versus 62%, respectively), the difference in signal between allografts and isografts, although significant for both, is more pronounced with the phagocytosis sensor. Taken together, fluorescence microscopy and flow cytometry illustrate how fluorescent nanoparticles facilitate better understanding of the exact cellular imaging signal source.

After evaluating the biological behavior of both probes during parenchymal rejection of heart grafts, we employed fluorescence tomography. This technique allows a volumetric reconstruction of the source of fluorescent light in the intact, living animal [10]. In our study, FMT enables the in vivo detection of protease activity, deploying a 3D map of macrophage function. Compared to the prevailing standard of histologic appearance, the protease activity detected by FMT correlates well with immunoreactive macrophage staining. High background signal caused by the biliary excretion of the phagocytosis sensor and lower average target signal intensities explain in part the difficulties of detecting significant differences in FMT signals between iso- and allografts heterotopically implanted in the abdominal cavity. We overcame this problem with magnetic resonance imaging of phagocytosis sensor uptake, which provides superior spatial resolution and soft tissue contrast.

Magnetic nanoparticles detect rejection by MRI, serving either as blood pool agents for perfusion imaging [18] or in delayed MRI [19-21]. Comparable to previous studies, magnetic resonance imaging resolved higher phagocytosis sensor uptake in allografts. No significant signal difference between allo- and isograft occurred 3 days after transplantation, when the inflammation resulting from the ischemia-reperfusion injury in both isograft and allograft predominates the effect of the gradually increasing alloimmune response in the allograft.

To evaluate the ability of the imaging approach to report on the severity of the immunologically mediated injury, we used cardiac transplantation into $RAG1^{-/-}$ mice recipients. These mice lack mature T and B lymphocytes [22] and totally mismatched allografts do not undergo rejection. Noninvasive macrophage-targeted imaging using either probe detected not only a gradual signal increase in allografts but also lower macrophage accumulation in hearts grafted into $RAG1^{-/-}$ recipients compared to B6 recipients. In addition, the signal measured by both FMT and MRI correlated with the prevailing standard of histologic appearance. Beyond demonstrating the ability of noninvasive imaging to report on the magnitude of the allogeneic immune response, these results illustrate the potential to study loss- or gain-of-gene functions by imaging in mice rather than in transplanted rat hearts as in previous reports [18-21, 23].

Iron oxide nanoparticles with comparable coatings to the preparation used in this study are already in clinical use (ferumoxides) or trials (ferumoxtran, ferumoxytol) for liver and macrophage-targeted imaging in cancer [24] and atherosclerosis [25]. Therefore, the MR imaging findings presented here should be readily translatable. Clinical FMT imaging is limited by depth, and given the physical limits is unlikely to cover the entire human heart. However, recent developments in catheter design allowed probing protease activity in vivo using intravascular access [26]. This approach might serve to guide biopsies in patients and so reduce the sampling error currently associated with fluoroscopically-guided procedures.

In conclusion, this study demonstrates the potential of quantitating myocardial MΦ content and function in vivo. The imaging tools described here could facilitate the search for new immunosuppressive and tolerogenic therapies, and its application might improve clinical graft surveillance.

## Supplementary Material

Refer to Web version on PubMed Central for supplementary material.

## Acknowledgements

The authors acknowledge the CMIR Mouse imaging program (Carlos Rangel, BS and Ann Yu, BS in MR imaging; Alexandra Kunin, BS in FMT and FRI) and the CMIR chemistry core (Nicolai Sergeyev, PhD) for assistance in the imaging and probe preparation and the CMIR pathology core (Yoshi Iwamoto, BS) for assistance in histology. We thank Elissa Simon-Morrissey for her managing skills and Joan Perry for editing the manuscript.

**Funding Sources:** This work was funded in part by the Donald W. Reynolds Foundation, the Translational Program of Excellence in Nanotechnology (TPEN) grant #U01HL080731, the American Heart Association Scientist Development Grant #0630010N (to K. Shimizu) and the American Society of Transplantation Basic Science Faculty Development Grant (to K. Shimizu).

## References

1. Mehra MR, Ventura HO, Chambers R, Collins TJ, Ramee SR, Kates MA, Smart FW, Stapleton DD. Predictive model to assess risk for cardiac allograft vasculopathy: an intravascular ultrasound study. J Am Coll Cardiol 1995;26:1537–1544. [PubMed: 7594082]
2. Soleimani B, Fu F, Lake P, Shi VC. Development of a combined heart and carotid artery transplant model to investigate the impact of acute rejection on cardiac allograft vasculopathy. J Heart Lung Transplant 2008;27:450–456. [PubMed: 18374883]
3. Tan CD, Baldwin WM 3rd, Rodriguez ER. Update on cardiac transplantation pathology. Arch Pathol Lab Med 2007;131:1169–1191. [PubMed: 17683180]
4. Shimizu K, Libby P, Shubiki R, Sakuma M, Wang Y, Asano K, Mitchell RN, Simon DI. Leukocyte integrin Mac-1 promotes acute cardiac allograft rejection. Circulation 2008;117:1997–2008. [PubMed: 18378617]
5. Wyburn KR, Jose MD, Wu H, Atkins RC, Chadban SJ. The role of macrophages in allograft rejection. Transplantation 2005;80:1641–1647. [PubMed: 16378052]
6. Nahrendorf M, Sosnovik DE, Waterman P, Swirski FK, Pande AN, Aikawa E, Figueiredo JL, Pittet MJ, Weissleder R. Dual channel optical tomographic imaging of leukocyte recruitment and protease activity in the healing myocardial infarct. Circ Res 2007;100:1218–1225. [PubMed: 17379832]
7. Sosnovik DE, Nahrendorf M, Deliolanis N, Novikov M, Aikawa E, Josephson L, Rosenzweig A, Weissleder R, Ntziachristos V. Fluorescence tomography and magnetic resonance imaging of myocardial macrophage infiltration in infarcted myocardium in vivo. Circulation 2007;115:1384–1391. [PubMed: 17339546]
8. Weissleder R, Tung CH, Mahmood U, Bogdanov A Jr. In vivo imaging of tumors with protease-activated near-infrared fluorescent probes. Nat Biotechnol 1999;17:375–378. [PubMed: 10207887]
9. Shaw SY, Westly EC, Pittet MJ, Subramanian A, Schreiber SL, Weissleder R. Perturbational profiling of nanomaterial biologic activity. Proc Natl Acad Sci U S A 2008;105:7387–7392. [PubMed: 18492802]
10. Ntziachristos V, Tung CH, Bremer C, Weissleder R. Fluorescence molecular tomography resolves protease activity in vivo. Nat Med 2002;8:757–760. [PubMed: 12091907]
11. Mahmood U, Tung CH, Bogdanov A Jr, Weissleder R. Near-infrared optical imaging of protease activity for tumor detection. Radiology 1999;213:866–870. [PubMed: 10580968]
12. Furukawa Y, Libby P, Stinn JL, Becker G, Mitchell RN. Cold ischemia induces isograft arteriopathy, but does not augment allograft arteriopathy in non-immunosuppressed hosts. Am J Pathol 2002;160:1077–1087. [PubMed: 11891204]
13. Shimizu K, Schonbeck U, Mach F, Libby P, Mitchell RN. Host CD40 ligand deficiency induces long-term allograft survival and donor-specific tolerance in mouse cardiac transplantation but does not prevent graft arteriosclerosis. J Immunol 2000;165:3506–3518. [PubMed: 10975872]
14. Akimoto H, McDonald TO, Weyhrich JT, Thomas R, Rothnie CL, Allen MD. Antibody to CD18 reduces neutrophil and T lymphocyte infiltration and vascular cell adhesion molecule-1 expression in cardiac rejection. Transplantation 1996;61:1610–1617. [PubMed: 8669106]
15. Stegall MD, Park WD, Kim DY, Covarrubias M, Khair A, Kremers WK. Changes in intragraft gene expression secondary to ischemia reperfusion after cardiac transplantation. Transplantation 2002;74:924–930. [PubMed: 12394832]
16. Baskin-Bey ES, Canbay A, Bronk SF, Werneburg N, Guicciardi ME, Nyberg SL, Gores GJ. Cathepsin B inactivation attenuates hepatocyte apoptosis and liver damage in steatotic livers after cold ischemia-warm reperfusion injury. Am J Physiol Gastrointest Liver Physiol 2005;288:G396–402. [PubMed: 15472011]
17. Nahrendorf M, Zhang H, Hembrador S, Panizzi P, Sosnovik DE, Aikawa E, Libby P, Swirski FK, Weissleder R. Nanoparticle PET-CT imaging of macrophages in inflammatory atherosclerosis. Circulation 2008;117:379–387. [PubMed: 18158358]

18. Johansson L, Johnsson C, Penno E, Bjornerud A, Ahlstrom H. Acute cardiac transplant rejection: detection and grading with MR imaging with a blood pool contrast agent--experimental study in the rat. Radiology 2002;225:97–103. [PubMed: 12354991]

19. Kanno S, Wu YJ, Lee PC, Dodd SJ, Williams M, Griffith BP, Ho C. Macrophage accumulation associated with rat cardiac allograft rejection detected by magnetic resonance imaging with ultrasmall superparamagnetic iron oxide particles. Circulation 2001;104:934–938. [PubMed: 11514382]

20. Penno E, Johansson L, Ahlstrom H, Johnsson C. Ultrasmall iron oxide particle contrast agent and MRI can be used to monitor the effect of anti-rejection treatment. Transplantation 2007;84:374–379. [PubMed: 17700163]

21. Wu YL, Ye Q, Foley LM, Hitchens TK, Sato K, Williams JB, Ho C. In situ labeling of immune cells with iron oxide particles: an approach to detect organ rejection by cellular MRI. Proc Natl Acad Sci U S A 2006;103:1852–1857. [PubMed: 16443687]

22. Mombaerts P, Iacomini J, Johnson RS, Herrup K, Tonegawa S, Papaioannou VE. RAG-1-deficient mice have no mature B and T lymphocytes. Cell 1992;68:869–877. [PubMed: 1547488]

23. Penno E, Johnsson C, Johansson L, Ahlstrom H. Macrophage uptake of ultra-small iron oxide particles for magnetic resonance imaging in experimental acute cardiac transplant rejection. Acta Radiol 2006;47:264–271. [PubMed: 16613307]

24. Harisinghani MG, Barentsz J, Hahn PF, Deserno WM, Tabatabaei S, van de Kaa CH, de la Rosette J, Weissleder R. Noninvasive detection of clinically occult lymph-node metastases in prostate cancer. N Engl J Med 2003;348:2491–2499. [PubMed: 12815134]

25. Kooi ME, Cappendijk VC, Cleutjens KB, Kessels AG, Kitslaar PJ, Borgers M, Frederik PM, Daemen MJ, van Engelshoven JM. Accumulation of ultrasmall superparamagnetic particles of iron oxide in human atherosclerotic plaques can be detected by in vivo magnetic resonance imaging. Circulation 2003;107:2453–2458. [PubMed: 12719280]

26. Jaffer FA, Vinegoni C, John MC, Aikawa E, Gold HK, Finn AV, Ntziachristos V, Libby P, Weissleder R. Real-time catheter molecular sensing of inflammation in proteolytically active atherosclerosis. Circulation 2008;118:1802–1809. [PubMed: 18852366]

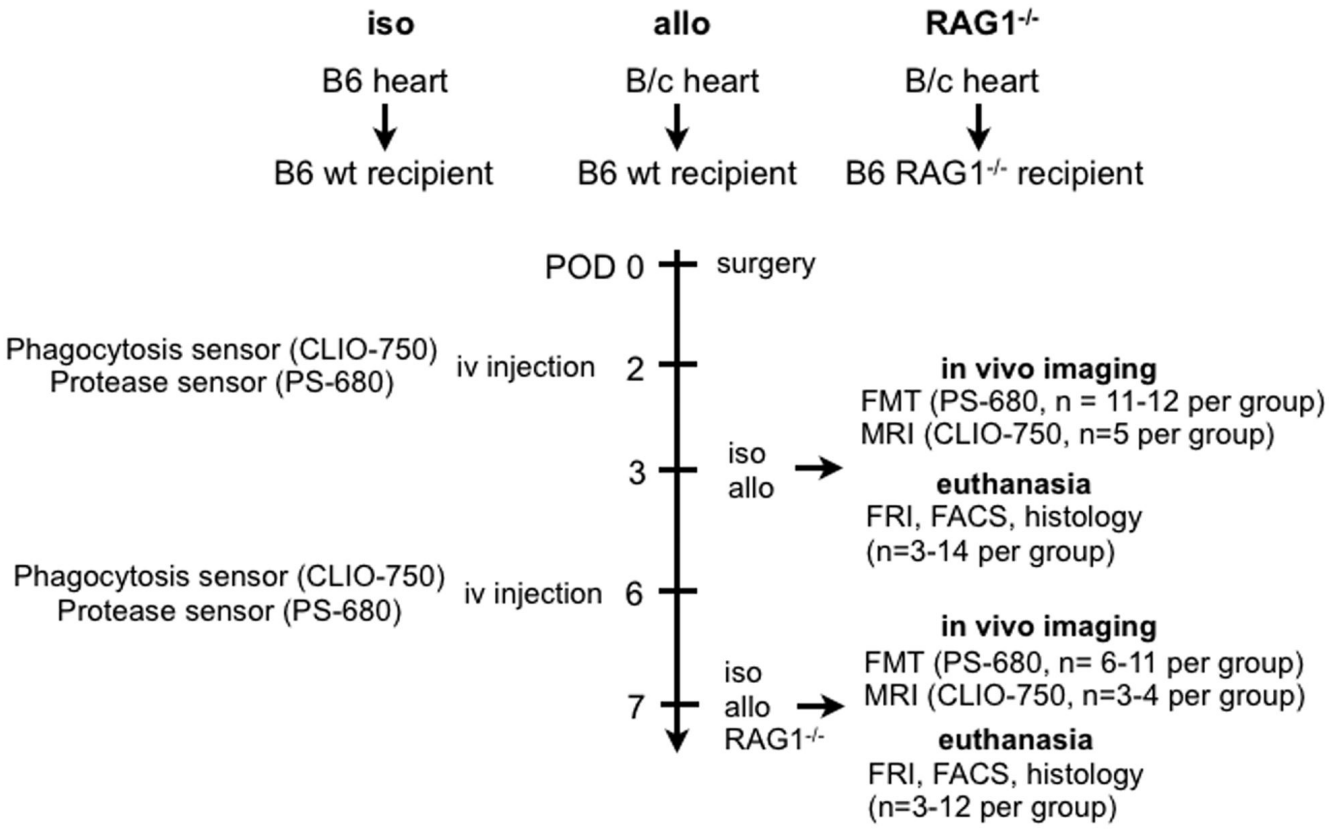


**Figure 1. Experimental design**

This study included three different groups of animals: isograft recipients (iso), allograft recipients (allo), and RAG1-/- allograft recipients (RAG1-/-). At POD 2 or 6 all operated animals with a functional heart graft received the imaging probes. Twenty-four hours after probe injection, the mice underwent in vivo imaging: fluorescence molecular tomography (FMT) after protease sensor injection, and MR imaging after phagocytosis sensor injection. Thereafter, we euthanized the animals and produced myocardial rings from the donor hearts to conduct fluorescence reflectance imaging (FRI). Also, samples from the transplants underwent flow cytometric (FACS) and histological analyses.

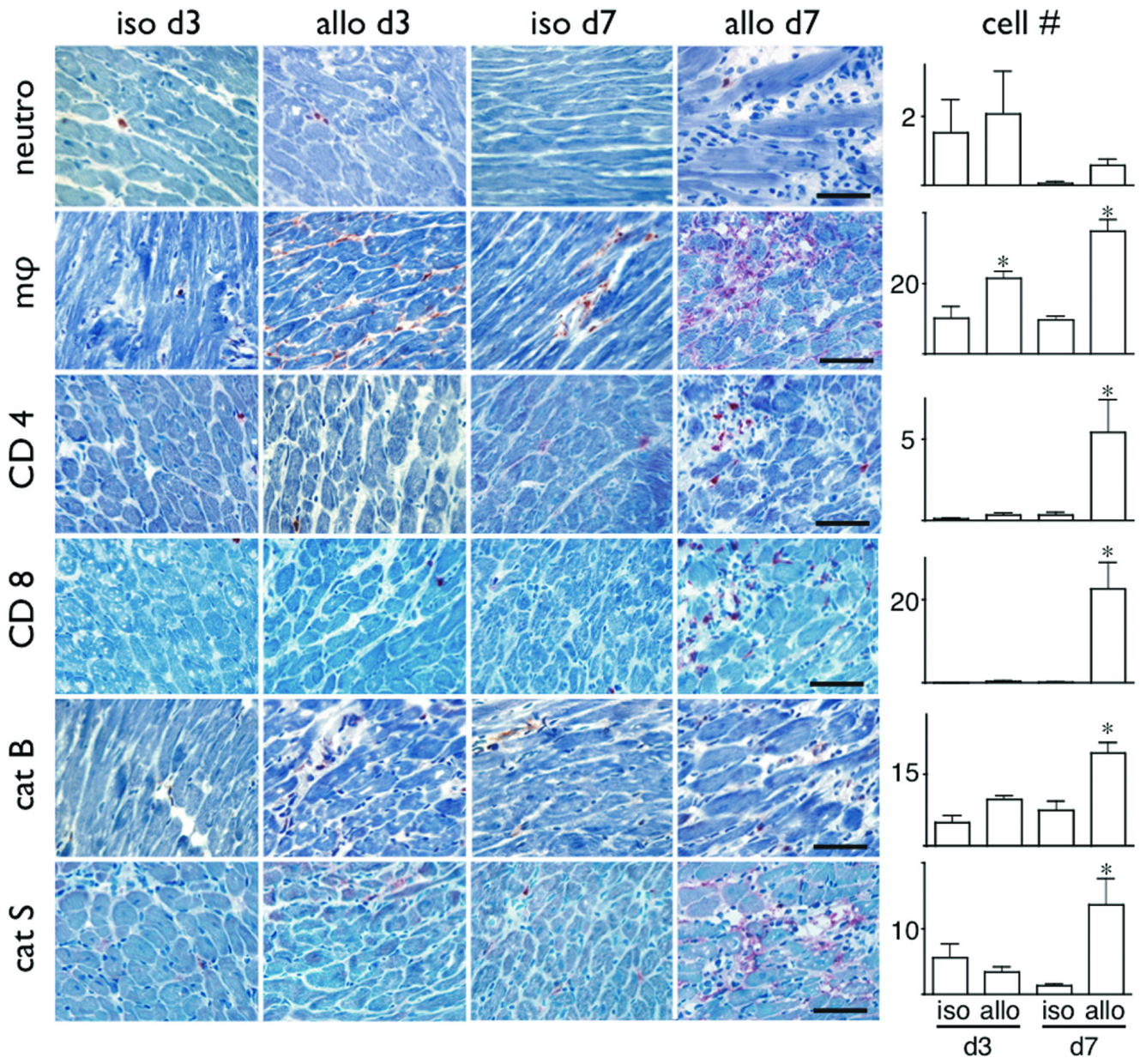


**Figure 2. Macrophages and cathepsin-positive cells accumulate predominantly in the allograft**

Representative sections stained with anti-mac3, anti-NIMP-R14, anti-CD4, anti-CD8, anti-cathepsin B, and anti-cathepsin S are shown for isografts and allografts at POD 3 and 7. The bar graphs present the mean number of positive cells per high power field. For macrophages and cathepsins B and S, the allograft had more positive cells than did the isograft at POD 7. At POD 3, allografts had more macrophage accumulation than did isografts, and in allografts the number of macrophages increased from POD 3 to POD 7. (Magnification ×400, Bar=40 μm)

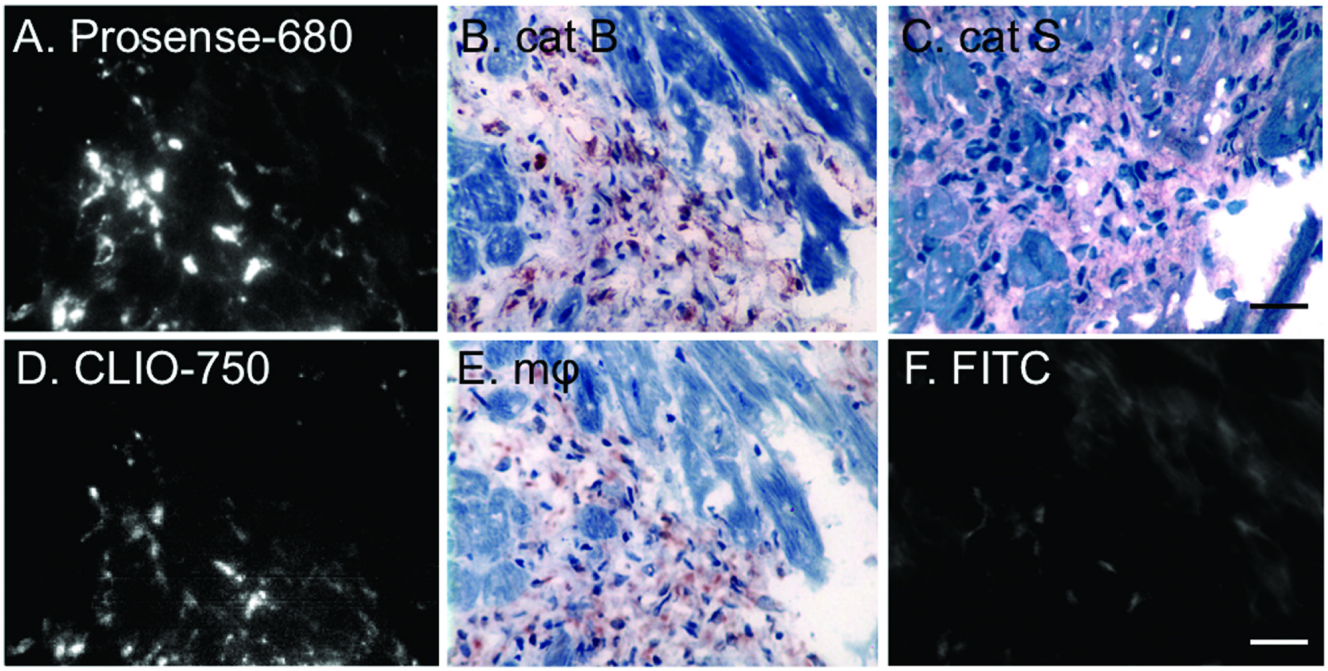


**Figure 3. Fluorescent microscopy illustrates that signal of both protease sensor and phagocytosis sensor colocalizes with immunoreactive macrophages as well as with cathepsins B and S**

A, D, F, Fluorescence microscopy was performed at different wavelengths on same section of heart grafts. A, In the channel permitting emission of activated Prosense-680 only, fluorescence colocalized with positive staining for cathepsins B and S as well as with macrophages in adjacent sections (B, C and E, respectively). D, In the channel for the phagocytosis sensor emission, the resulting fluorescent signal colocalized with positive staining for macrophages (E). F, The image acquisition in the FITC channel indicates that autofluorescence contributes little to the signal in A and D. (Magnification ×400, bar=40 μm.)

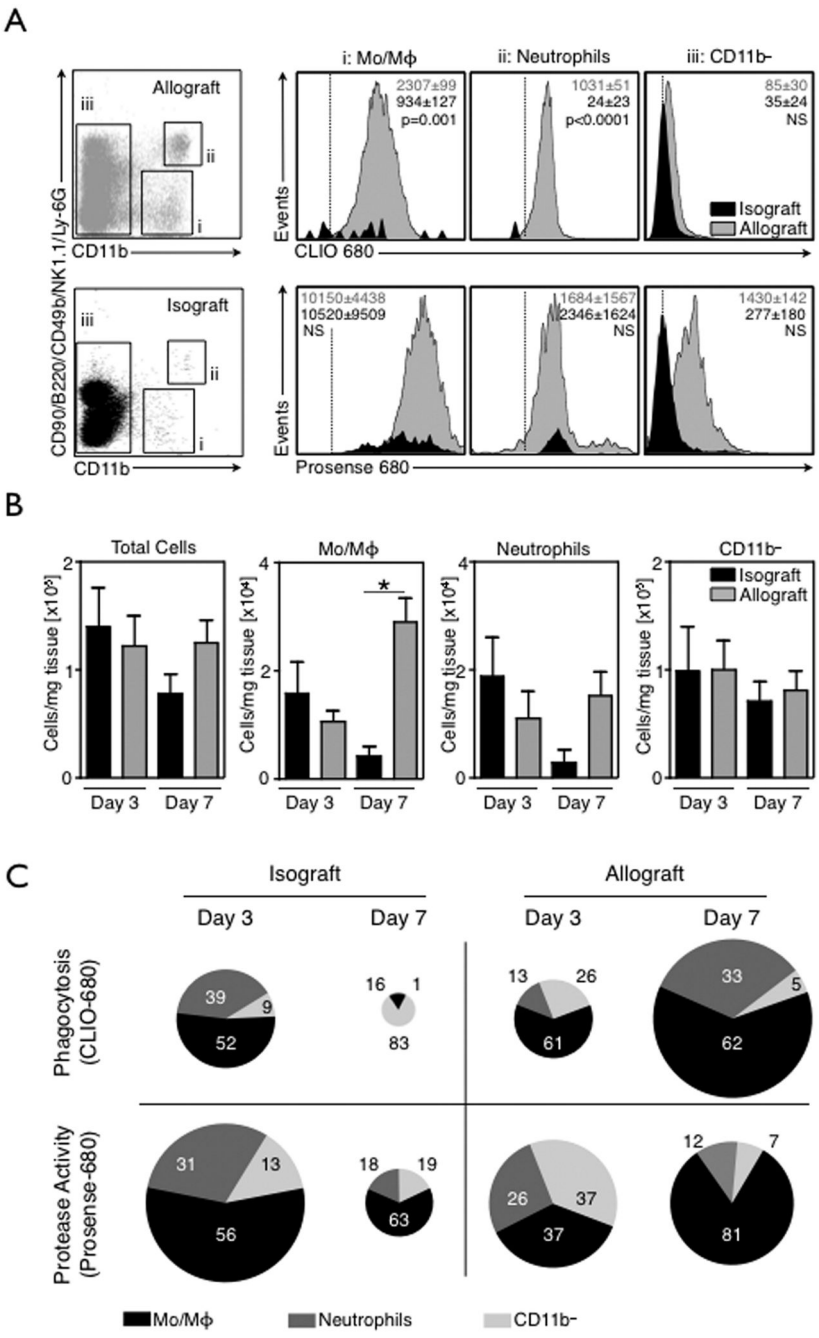


**Figure 4. Flow cytometry shows that monocytes/macrophages predominantly contribute to the imaging signal**

A, Dot plots show living cells from allografts (gray) and isografts (black) stained with CD11b and CD90/B220/CD49b/NK1.1/Ly-6G. Cells were identified as monocytes/mφ (gate i), neutrophils (gate ii), and CD11b- cells (including lymphocytes) (gate iii). For each cell population, representative histograms depict the fluorescence intensities of the phagocytosis sensor (CLIO 680) and the protease sensor (Prosense 680) in both allografts (gray) and isografts (black). The number of dots and the height of the histogram peaks illustrate the difference in cell number/mg tissue retrieved from allografts and isografts on POD 7. A negative control for each cell population (animal not injected with sensor), shown as a dashed vertical line,

demarcates the border between autofluorescence and positive signal. Mean fluorescent intensities (MFI) ± SD are shown. (NS = not significant).

B, Bar graphs display the cell number per mg tissue, calculated as total cell numbers/mg tissue multiplied by % of gated population. Statistical analysis for each cell type was performed with one-way ANOVA with Tukey's Multiple Comparison Test, *$P < 0.001$.

C, Relative contribution to the overall fluorescence for each cell population. Pie chart area corresponds to mean total imaging signal (calculated as cell number/mg that is positive for the sensor). Relative contribution of each cell population is shown as percentage of overall signal and pictorially represented by the magnitude of each slice. Monocyte/macrophages dominated as a cellular contributor to the fluorescence signal.

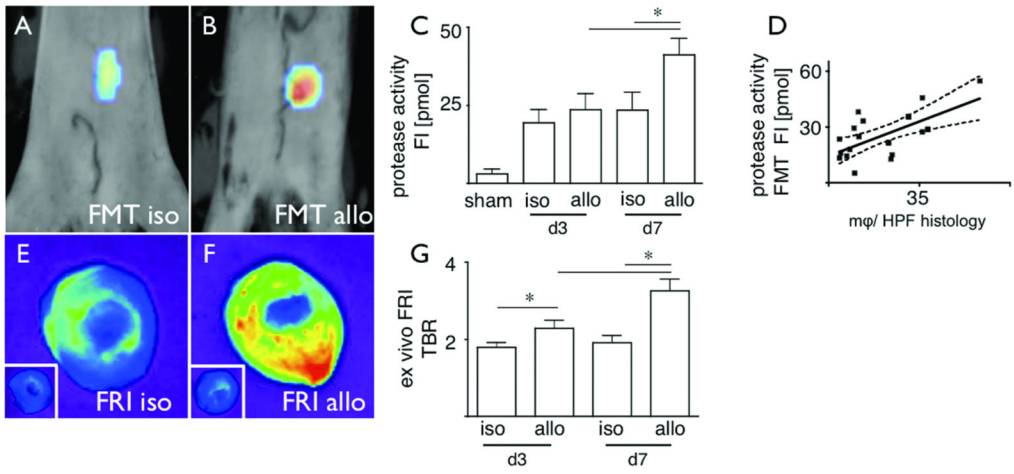


**Figure 5. In vivo fluorescence molecular tomography (FMT) demonstrates higher protease activity in the allograft than in the isograft of mice injected with protease sensor**

A and B, FMT after injection of protease sensor at POD 7, with the signal representing the quantity of fluorescence. A, The FMT signal in the isograft indicated continuing ischemia reperfusion injury. B, In the allograft, the FMT signal exceeded that in the isograft, reflecting the inflammatory response due to the alloimmune reaction. C, The quantity of fluorescence detected in the volume of interest is given in pmol. The fluorescence was 7-10-fold higher in heart grafts than in sham-operated mice (n=3), and graft rejection resulted in a significant difference between the isograft and allograft at POD 7. Additionally, fluorescence increased in allografts from POD 3 to POD 7. D, Fluorescence in pmol detected by FMT at POD 3 and 7 in isografts and allografts correlates with numbers of immunoreactive macrophages ($R^2$=0.42, p=0.0014). E and F, Validation of in vivo imaging using FRI after injection of protease sensor at POD 7, with the signal representing counts per pixels. E, The signal in the isograft was significantly higher than in the native heart (inset shows native heart of same animal), indicating an ongoing ischemia reperfusion injury. F, The signal in the allograft was not only higher than in the native heart (inset shows native heart of same animal) but also higher than in the isograft (E). G, The target-to-background ratio (TBR) was calculated from the counts per pixels of heart grafts normalized to the counts of native hearts. A significant difference of the TBR between isograft and allograft at POD 7 and an increase in TBR in allografts from POD 3 to POD 7 confirmed the in vivo findings (A-C). Additionally, allografts had higher TBR than isografts at POD 3.

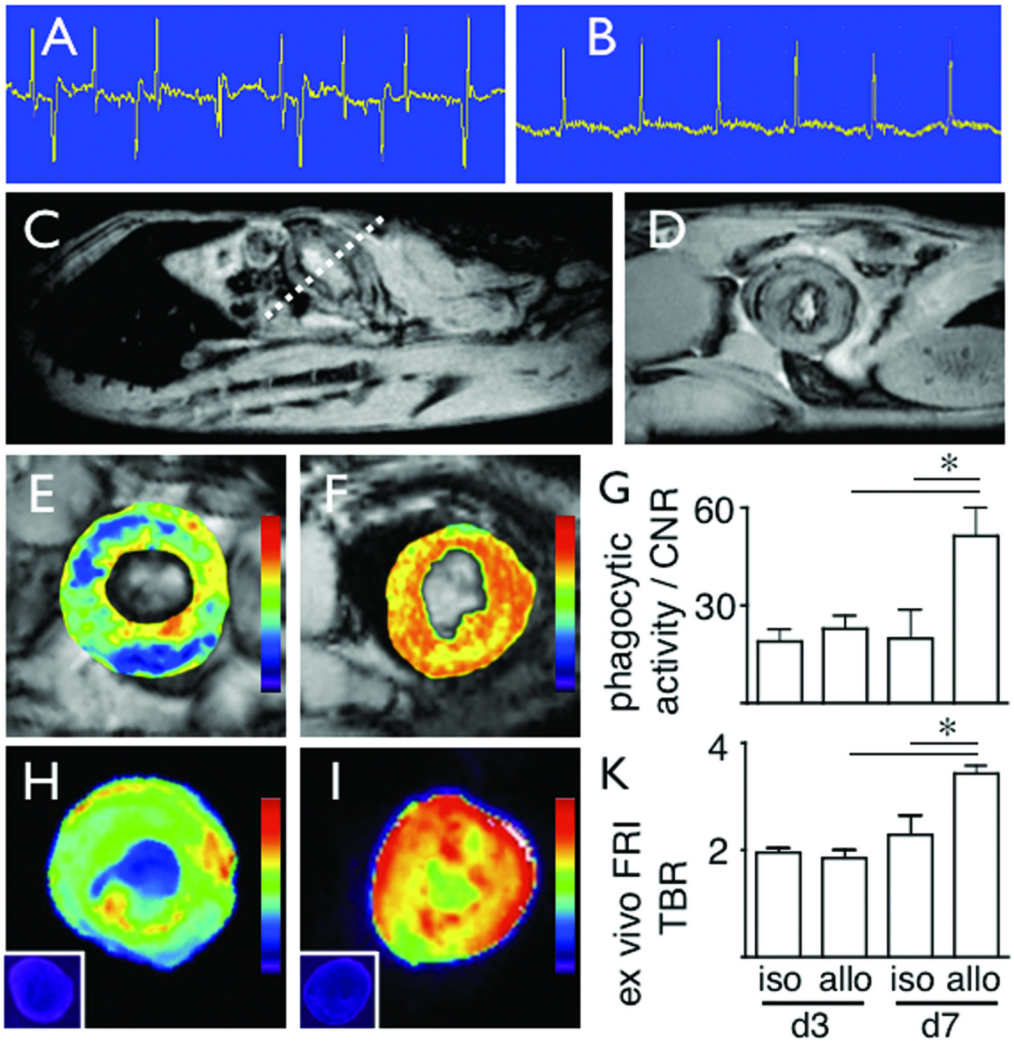


**Figure 6. Combined MRI and fluorescence reflectance imaging (FRI) reveals higher phagocytic activity in the allograft than in the isograft of mice injected with phagocytosis marker**

A, Electrocardiogram (ECG) with electrodes on front and back paws shows QRS complexes and comparable heart rates of both native and transplanted hearts. However, this combined trace would not allow triggering MRI acquisition to the graft. B, ECG with electrodes attached to hind limbs reports activity of transplanted heart only. C, Long axis view of the transplanted heart in an intra-abdominal location, with the dotted line indicating the position of the short axis view in D. E through G, T2*-weighted MRI after phagocytosis sensor injection resulted in negative signal enhancement in the grafted heart, with the signal represented as contrast-to-noise ratio (CNR). E and F, At POD 7, the contrast was stronger in the allograft (F) than in the isograft (E). G, Quantitatively, the CNR was significantly higher in allografts than in isografts at POD 7, and the CNR increased in allografts from POD 3 to POD 7. H through K, FRI after phagocytosis sensor injection validates in vivo imaging. H, The isograft exhibited a considerably higher signal than the native heart (inset shows native heart of same animal), pointing to ongoing ischemia reperfusion injury. I, The signal in the allograft was higher than in the native heart (inset shows native heart of same animal) and also higher than in the isograft (H) at POD 7. K, The target-to-background ratio (TBR) was calculated from the fluorescence of heart grafts normalized to the native hearts. A significant difference of the TBR between

isograft and allograft at POD 7 as well as an increase in TBR in allografts from POD 3 to POD 7 corroborate the in vivo findings (E-G).

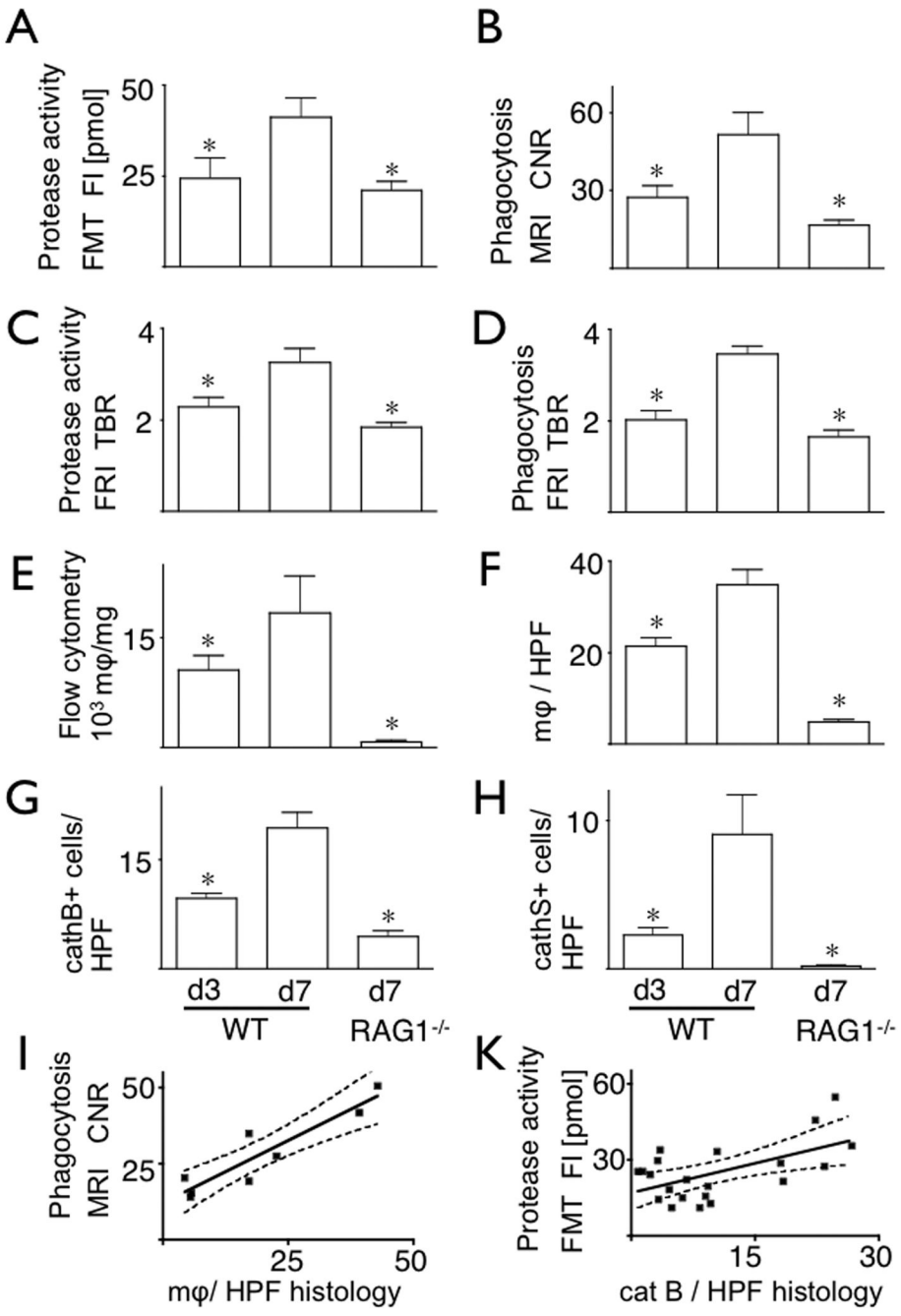


**Figure 7. In vivo FMT and MRI detect increasing protease and phagocytic activity in allografts as well as attenuated rejection in allografts of immunodeficient hosts**

A, The fluorescence (pmol) detected by in vivo FMT increased in allografts of B6 wild-type recipients from POD 3 to POD 7 and decreased in RAG1$^{-/-}$ recipients compared to B6 wild-type recipients at POD 7, illustrating the ability of the FMT to detect the severity of the rejection. B, The contrast-to-noise ratio (CNR) resulting from the negative signal enhancement detected by MRI intensified in grafts of B6 wild-type recipients from POD 3 to POD 7 and diminished in RAG1$^{-/-}$ recipients compared to B6 wild-type recipients at POD 7. C and D, FRI confirmed the in vivo imaging findings that the fluorescence intensity of the heart graft normalized to native heart in the same animal (target-to-background ratio = TBR) increased

in B6 wild-type allograft recipients with time and diminished in the $RAG1^{-/-}$ allograft recipients at POD 7 after protease sensor (C) and phagocytosis marker (D) injection. E, Flow cytometry corroborated imaging findings revealing a gradually increasing number of macrophages in allografts and a substantially reduced number of macrophages in $RAG1^{-/-}$ allograft recipients compared to B6 wild-type recipients at POD 7. The number of monocyte/macrophages per mg tissue was calculated as total cell numbers/mg tissue multiplied by % of gated monocyte/macrophage population. F-H, The number of cells per high-magnification field that were positive for a macrophage marker (F), cathepsin B (G), and cathepsin S (H) increased in allografts with time and were lower in $RAG1^{-/-}$ allograft recipients than in B6 wild-type recipients at POD 7. I and K, Detection of phagocytosis by MRI correlated with the number of macrophages as assessed by histology (I, $r^2=0.85$, $p=0.001$), and in vivo protease activity correlated with cellular staining of cathepsin B (K, $r^2=0.33$, $p=0.006$). Correlations included allografts in B6 wild-type recipients on POD 3 and 7 and RAG1-/- recipients on POD 7.